Oncogene (2004) 23, 5543–5550

www.nature.com/onc

SHORT REPORTS

Versatile analysis of multiple macromolecular interactions by SPR imaging: application to p53 and DNA interaction

Emmanuel Maillart[1,4], Karen Brengel-Pesce[2,4], Delphine Capela[3], André Roget[2], Thierry Livache[2], Michael Canva[1], Yves Levy[1] and Thierry Soussi*[,3]

[1]*Laboratoire Charles Fabry de l'Institut d'Optique (LCFIO), Centre National de la Recherche Scientifique CNRS UMR 8501, Bât. 503, Université Paris XI, 91403 Orsay, France;* [2]*CREAB, UMR 5819 (CEA, CNRS, UJF), Département de Recherche Fondamentale sur la Matière Condensée, 17 rue des Martyrs, 38054 Grenoble, France;* [3]*Laboratoire de génotoxicologie des tumeurs, EA 3493 UPMC-IC, Hôpital tenon, Pneumologie, 4 rue de la Chine, 75019 Paris, France*

The greatest challenge in the postgenomic era is the description of proteome interactions, such as protein–protein or protein–DNA interactions. Surface plasmon resonance (SPR) is an optical technique in which binding of an analyte to the surface changes the refractive index at the surface/solution interface. Molecular interactions are analysed in real time without a labeling step. Currently, the limit to SPR imaging is the small number of reactions that can be simultaneously analysed. Using a novel grafting technology and a new imaging system, we increased the throughput of SPR imaging. The interaction between p53 and DNA was chosen as a paradigm for validation of this assay. Using a tagged DNA methodology, we simultaneously targeted multiple DNA sequences on a single chip. The interaction between p53 and these DNA sequences was monitored by SPR imaging. Qualitative and quantitative analysis provides results similar to those obtained with conventional technologies.

Oncogene (2004) **23,** 5543–5550. doi:10.1038/sj.onc.1207639
Published online 7 June 2004

Keywords: p53 tumor suppressor gene; DNA binding; SPR imaging; EMSA; polypyrrole

Detection of DNA binding activity is predominantly performed by several gel-based assays, such as electrophoretic mobility shift assay (EMSA) (Fried and Crothers, 1981) or DNA footprinting (Galas and Schmitz, 1978). These methods are not adapted to high-throughput formats, require labeling, usually with a radioisotope, and are end point methods that do not allow kinetic analysis. Surface plasmon resonance (SPR) imaging is a label-free, surface-sensitive spectroscopic technique that can be used to detect the binding of DNA, RNA, and proteins onto arrays of probe biomolecules covalently attached to chemically modified gold surfaces (Rich and Myszka, 2000). Our previous work focused on the creation and characterization of robust surface chemistries for the attachment of various biomolecules onto chemically modified gold surfaces with a novel methodology based on polypyrrole-based surface functionalization (Guedon *et al*., 2000). We also showed that multispot parallel DNA hybridization and denaturation could also be detected (Livache *et al*., 2003), unlike the commercially available instruments that are limited to four channel detection.

p53 activation in response to a stress leads to the transcription of numerous genes that contain one or two p53 recognition sites in either their promoter or intronic sequences (Vogelstein *et al*., 2000).

The interaction with DNA is certainly one of the most important, but also one of the least well-known activities of the p53 protein, as, in contrast with other transcription factors, the recognition site is extremely degenerated (El-Deiry *et al*., 1992; Kim and Deppert, 2003). None of the p53 target genes identified to date contains the same sequence (Tokino *et al*., 1994). This heterogeneity could at least partially account for the variability of the p53 response as a function of the type or intensity of stress. It is highly probable that this response is also modulated by other cellular proteins. The situation is made even more complex by the discovery of other members of the p53 family, that is, p63 and p73 (Melino *et al*., 2002). These proteins are also able to recognize the same regulation sequence as p53 with an activating or inhibitory effect depending on the isoform. These proteins therefore present a potential for complex positive and negative transcriptional regulation, the biological significance of which remains unknown. The interaction capacities of mutant p53 with DNA are also complex and have been insufficiently investigated. First of all, there is a very marked heterogeneity of loss of function of mutant p53 in terms of their capacity to recognize certain transcription promoters, resulting in different transactivation activities. The best known example is that of the H175P mutant, which no longer recognizes the transcription

*Correspondence: T Soussi;
E-mail: thierry.soussi@tnn.ap-hop-paris.fr
[4]These authors contributed equally to this study
Received 11 November 2003; revised 2 February 2004; accepted 17 February 2004; published online 7 June 2004

promoters of apoptotic genes such as bax, but recognizes that of the antiproliferative gene p21 (Friedlander *et al*., 1996; Rowan *et al*., 1996). Several recent studies have shown that the majority of mutant p53 proteins presents varying degrees of residual transactivation activity, which could account for the great phenotypic diversity of the behavior of tumors in response to therapy (Kato *et al*., 2003; Resnick and Inga, 2003). It has also been shown that some mutant p53 proteins could acquire the capacity to recognize new DNA sequences, such as nuclear matrix attachment region sequences (MARs) (Muller *et al*., 1996; Deppert *et al*., 2000). In order to validate this high-throughput SPR imaging approach to a biological problem, we used this technique to simultaneously study the interactions between p53 and five different DNA sequences. We chose three response elements found in p53-induced genes (WAF1, mdm2, and bax) that have been shown by gel shift assay to have different p53 binding activities (Figure 1). The other sequence BB9 corresponds to a wild-type (wt) consensus sequence previously shown to strongly bind to p53 (Halazonetis *et al*., 1993), whereas BB9M is a mutated sequence used as a negative control (Table 1).

To increase the versatility of this assay, we used a modification of the Zip-code strategy developed by Gerry *et al*. (1999). The gold layer was functionalized by polymerization of a mix of pyrrole and single-stranded oligonucleotide probes containing a pyrrole residue on the 5′ end (Zip-Pyr) (Figure 2). Each zip-code sequence is composed of a 24-mer sequence composed of six tetramers designed to prevent any cross-hybridization between the various sequences (Table 1). The number of possible zip-codes can be easily increased and they have been previously used for high-throughput detection of p53 (Dong *et al*., 2001), ras (Dong *et al*., 2001), or BRCA1 (Favis *et al*., 2000) mutations. The target sequence is a partial duplex DNA with a single-strand sequence complementary to a specific zip-code and a duplex section containing the p53 binding site (Table 1). This strategy presents several advantages. Firstly, target DNA can be removed either by heating or with alkaline buffer so that the chip can be used several times. This reaction can be easily monitored by SPR. Secondly, the

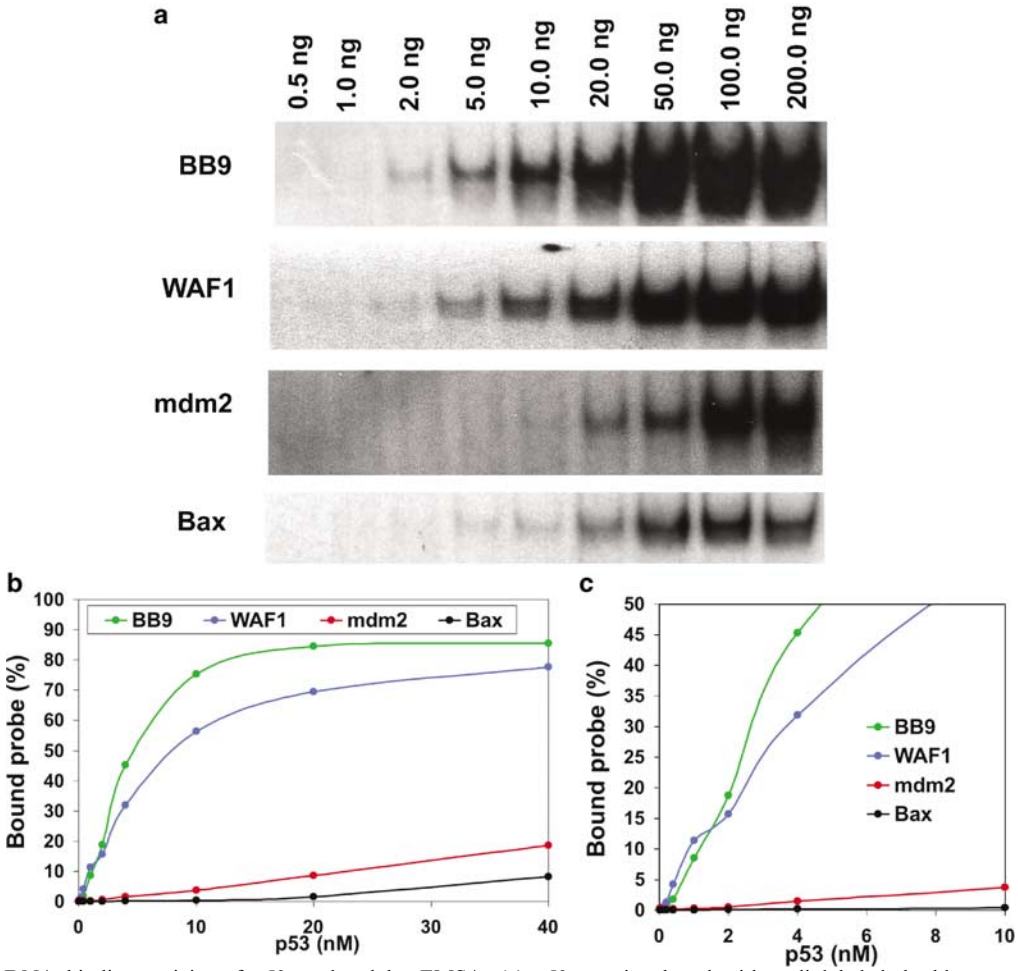

Figure 1 DNA binding activity of p53 analysed by EMSA. (**a**) p53 was incubated with radiolabeled double-stranded probes containing the BB9 (consensus), WAF1, mdm2, or Bax binding sites, as described in Experimental protocol. Bound and free probes were separated by gel electrophoresis and were quantified by phosphoimaging (The apparently higher DNA binding activity of p53 to bax is due to overexposure of the autoradiogram. This does not affect the ratio between bound and free probe). (**b**) Quantification of the analysis shown in (**a**). (**c**) Partial view of (**b**) indicating the values obtained with a small amount of p53 protein

Table 1 DNA probes and targets

Zip 9	5′ Pyr-T(10)-	GACCATCGTGCGGGTAGGTAGACC	3′
	5′	GGGCATGTCCGGGCATGTCC	3′
cZC9BB9	3′	CTGGTAGCACGCCCATCCATCTGGCCCGTACAGGCCCGTACAGG	5′
Zip 2	5′ Pyr-T(10)-	CAGCACCTGACCATCGATCGCAGC	3′
	5′	GAACATGTCCCAACATGTTG	3′
cZC2WAF1	3′	GTCGTGGACTGGTAGCTAGCGTCGCTTGTACAGGGTTGTACAAC	5′
Zip 6	5′ Pyr-T(10)-	GACCGGTATGCGACCTGGTATGCG	3′
	5′	GGTCAAGTTCAGACACGTTC	3′
cZC6MDM2	3′	CTGGCCATACGCTGGACCATACGCCCAGTTCAAGTCTGTGCAAG	5′
Zip 7	5′ Pyr-T(10)-	TGCGATCGCAGCGGTAACCTGACC	3′
	5′	TCACAAGTTAGAGACAAGCCT	3′
cZC6BAX	3′	ACGCTAGCGTCGCCATTGGACTGGAGTGTTCAATCTCTGTTCGGA	5′
Zip 4	5′ Pyr-T(10)-	TGCGGGTACAGCACCTACCTTGCG	3′
	5′	GGGCAGGACCGGGCAGGACC	3′
cZC4BB9M	3′	ACGCCCATGTCGTGGATGGAACGCCCCGTCCTGGCCCGTCCTGG	5′

The zip oligonucleotide used as the surface bound probe contains a pyrrole residue at the 5′ end for grafting to the gold layer functionalized surface. It is followed by a series of 10 T residues to facilitate the accessibility of the zip sequence. Zip sequence and numbering are taken from Gerry *et al*. (1999). The target sequences contain a partial single strand sequence complementary to a specific zip-code sequence followed by a 20 bp duplex sequence corresponding to the p53 binding site. The WAF1 (5′ response element), mdm2, and bax sequence are of human origin. BB9 is a consensus sequence deduced from a comparison of all p53 binding sites. It binds p53 with a high affinity. BB9M is a derivative of BB9 mutated at four conserved residues (underlined) and is used as a negative control. The target sequence was produced by hybridization of equimolar amounts of the short and long oligonucleotides (final concentration: 10 μM) in water

double-strand sequence of the target can contain any DNA binding sequence for any ligand (protein or other), as the specificity of binding to the chips is defined by the single strand sequence complementary to the zip-code.

As shown in Figure 2, the experiment can be divided into three steps. In the first step, the surface is prepared by grafting various Zip-Pyr probes at defined locations on the gold surface. In step 2, the DNA binding sequences are hybridized to these specific locations on the chip. In step 3, p53 protein is injected onto the chip and simultaneous monitoring of the interaction with DNA on the entire chip is performed by SPR imaging (Supplementary Figure 1 online). Preliminary fluorescence experiments were performed to detect the efficiency and specificity of target hybridization to their corresponding probes (Figure 3a and b) and for p53 DNA binding activity (Figure 3c and d). Zip-codes were originally defined and optimized for hybridization at 72°C. Using labelled (fluorescence, data not shown) and unlabelled (SPR, Supplementary Figure 2 online) target sequences, we showed that no cross-hybridization occurred between the various probes and targets at room temperature. DNA binding activity was monitored by the detection of p53 with a specific monoclonal antibody (DO7) labeled with biotin and identified by fluorescence with streptavidin-phycoerythrin. Efficient binding to BB9 and, to a lesser extent, to WAF1 was detected but no significant interaction could be detected with the other probes (mdm2 and bax) (Figure 3c and d). No nonspecific interaction was detected with either the BB9M probe, the gold surface, or free pyrrole, indicating that the p53 protein has no significant nonspecific binding activity in this assay. The higher binding of p53 to BB9 compared to WAF1 was expected from the EMSA study (Figure 1) and indicates that this experimental design can quantify the protein–DNA interaction. This fluorescence-based assay is an end point measure that does not allow kinetic analysis. Furthermore, no interaction of p53 with mdm2 and bax target could be detected prompting us to check whether SPR could provide better sensitivity.

SPR imaging allows direct monitoring and control of both step 2 (hybridization of targets to their corresponding probes) and step 3 (p53 interaction with DNA). Monitoring of step 2 allows direct quantification of the amount of target that hybridizes to each probe and the plateau of the curve indicates that all probes have been hybridized with their corresponding target (Figure 4c and d). From the reflectivity variations (measured with $a \pm 0.02\%$ precision) and the molar weight of the dsDNA ($M = 19.2$ kDa), we were able to deduce the dsDNA density on each spot (or the average distance d between two molecules). These densities were 24.5 fmol/mm^2 ($d = 8.2$ nm), 21.5 fmol/mm^2 ($d = 8.8$ nm), 17.7 fmol/mm^2 ($d = 9.7$ nm), and 12.4 fmol/mm^2 ($d = 11.6$ nm) for the 2, 1, 0.5, and 0.25 μM probe concentrations, respectively. No decrease of target binding was detected at high probe concentrations and the efficiency was similar for each type of probe (compare Figure 3 and 5a). Although it could be theoretically possible to use higher probe concentrations to increase the uptake of p53, we used a low concentration to avoid steric hindrance that could occur during the interaction of activated p53 (MW around 500 kDa if we assume that two activating antibodies are bound to p53) and DNA.

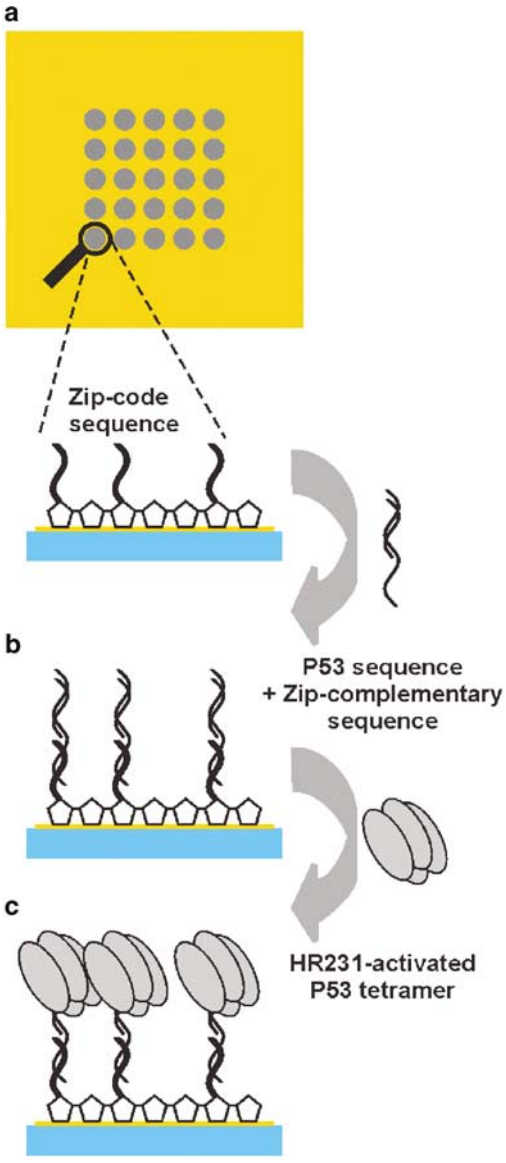

Figure 2 Plan of the SPR strategy for detection of p53 DNA binding activity. In step 1, the gold-coated prism is functionalized at different specific locations in the form of circular spots. On each spot, the specific single-strand zip-code oligonucleotide linked to a pyrrole residue (the probe) is electropolymerized on the gold surface by the methods described by Guedon *et al*. (2000) leading to covalent binding on the chips. Some spots were created with free pyrrole used as negative control. Although in the current study, only 25 different spots were used, the number of spots can be increased by decreasing their size. In step 2 (from **a** to **b**), a mix containing the various p53 target sequences, each one containing a single-strand tail complementary to a specific zip-code, is hybridized on the chip leading to the active chip (shown for one spot in the figure). In step 3 (from **b** to **c**), the p53 protein is injected on the surface of the chip where it can simultaneously interact with the various p53 binding sites. These interactions are monitored by SPR as described in Supplementary Figure 1 online

In step 3, injection of p53 leads to clear detection of protein binding to the BB9 and WAF1 sequences, and a lower but significant signal with mdm2 (Figure 4e and f, also see Figure 5b and the movie as Supplementary Figure 3 online). Subsequent injection of a monoclonal antibody specific for p53 (DO7) led to an increase of signal only in spots that showed protein binding,

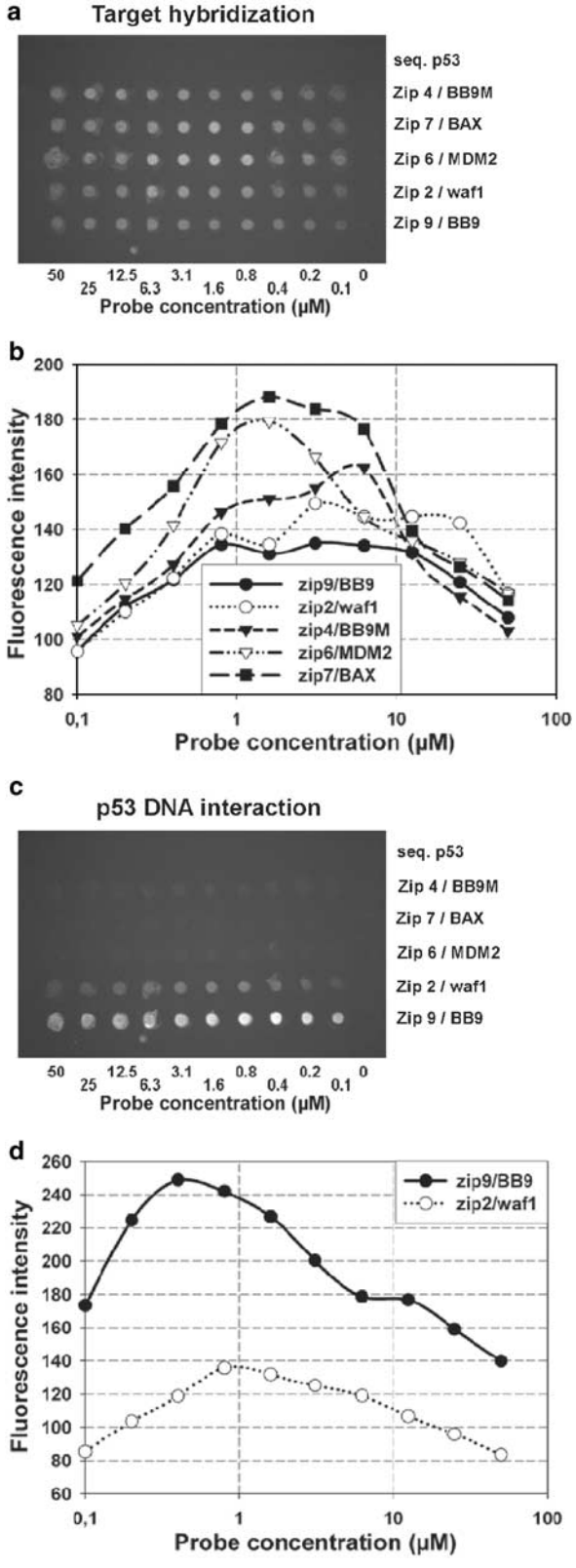

confirming that it is clearly p53 that binds to DNA (data not shown). Furthermore, control experiments in which p53 was not activated with HR231 did not lead to any significant p53 binding (data not shown).

Considering that p53 (46 kDa) activation occurred in an excess of HR231 (146 kDa), the molecular weight of the HR231-activated p53 tetramer is 476 kDa and its size is approximately $32.5 \times 8\,nm^2$. From these values and the reflectivity variations, we obtained the surface coverage of the p53 protein: $3.3 \pm 0.25\,fmol/mm^2$ of p53 on BB9 spots ($d = 22.5 \pm 1$ nm) and $1.5 \pm 0.1\,fmol/mm^2$ of p53 on WAF1 spots ($d = 33.3 \pm 1$ nm). This difference is certainly due to the higher affinity of p53 for BB9 and the fact that the reactions did not occur at full equilibrium. The binding efficiency of p53 to DNA was better when using a low probe density (see Figure 5b). In view of the average distance between the target DNA strands and the size of the p53 complex, the tetramer, when bound to a DNA target, masks three to four other targets, indicating that the saturating binding efficiency is about 20% for the 2 μM probe concentration and 25% for the 0.25 μM probe concentration. At low probe density, p53 nearly saturated the target DNA layer. This result shows that lateral accessibility of the dsDNA target is necessary for p53 recognition.

The exponential fitting of the association part and the dissociation part of each kinetic curve allows determination of the dissociation constant of the BB9/p53 complex (apparent $K_D = 0.9 \pm 0.5$ nM) and the WAF1/p53 complex (apparent $K_D = 3.5 \pm 1.5$ nM) for an injected p53 concentration of 2.1 nM. These values indicate that the affinity of p53 for BB9 is three to five times higher than the affinity of p53 for WAF1. The value for WAF1 is nearly similar to the K_D obtained by ultracentrifugation analysis (apparent K_D 0.83 ± 1.4 nM) (Balagurumoorthy *et al*., 1995).

Binding of p53 to mdm2 was too weak for any quantitative analysis. SPR was performed at a low p53 concentration (0.5–5.0 nM) and, at this concentration, EMSA did not detect any significant interaction with the

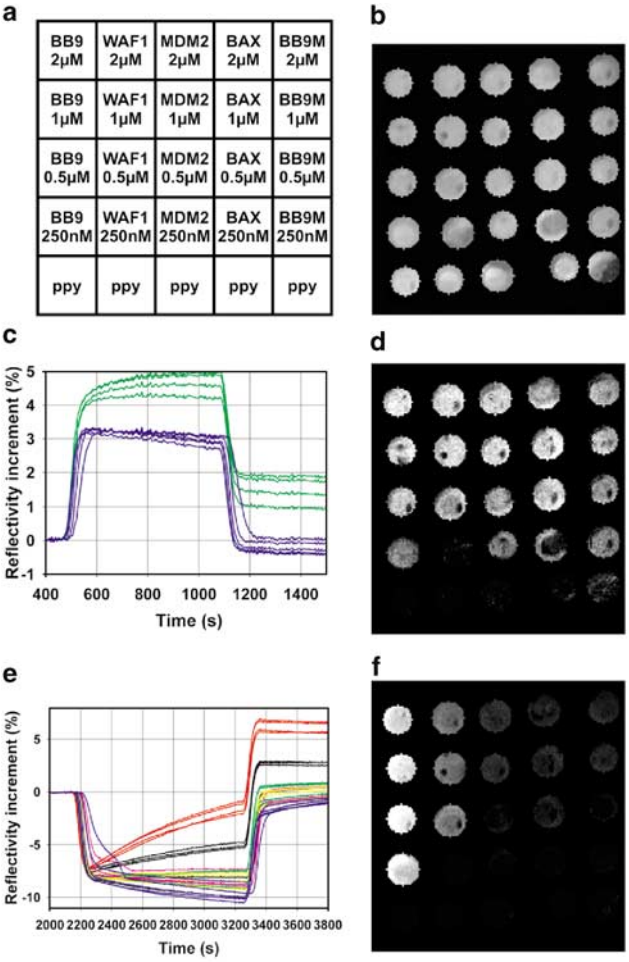

Figure 4 p53 DNA binding analysed by SPR. (**a**) Arrangement of the various spots on the gold layer of the functionalized matrix. Copolymerization was performed with a mix of 20 mM free pyrrole and various concentrations of oligonucleotide probes (ratios from 1/10 000 to 1/80 000). (**b**) SPR Imaging of the entire area in buffer before hybridization showing the signal in the various spots that contain the grafted zip sequence. In this image, the signal is mainly due to the polypyrrole film. Each spot is about 800 μm large and the distance between the centers of two spots is 1 mm. The black stripe in the bottom right corner is the border of the Teflon cell masking one nongrafted polypyrrole spot. (**c**) Hybridization kinetic of mdm2 target to its complementary sequence (zip6 spots, green) and the polypyrrole spots (blue). The initial baseline corresponds to the reflectivity level in the binding buffer. In this experiment, the five probes were injected simultaneously at $t = 400$ until 1000 s when buffer was injected. As expected, the amount of target DNA bound increased with the probe concentration. For hybridization, the final concentration of each target was 0.5 μM. (**d**) Image of the reflectivity increment caused by hybridization obtained from the difference between the images acquired at $t = 1500$ and 400 s. The WAF1 250 nM spot did not bind any DNA, suggesting no functionalization (this kind of problem cannot be seen in fluorescence microscopy). (**e**) Kinetics of the interaction of p53 with the various targets on all of the spots (Red: BB9, Black: WAF1, Green: mdm2, Yellow: bax, Pink: BB9M, Blue: ppy). After washing the cell with buffer, activated p53 was injected at $t = 2000$ until 3200 s. The gap in reflectivity between the buffer solution and the buffer + p53 solution is due to a small difference in their refractive index. Reactions were always stopped at 30 min in order to avoid problems associated with the natural heat-instability of wt p53 at room temperature (Hansen *et al*., 1996). (**f**) Image of the reflectivity increment caused by p53 binding obtained from the difference between the images acquired at $t = 3800$ and 2000 s. For (**b**), (**d**), and (**f**), a binary mask was applied for data analysis

Figure 3 Analysis by fluorescence (steps 2 and 3). (**a**) and (**b**) Target hybridization on a range of probe concentrations. (**a**) Photograph of the slide after hybridization. (**b**) Quantification analysis of the slides shown in (**a**). In this experiment, equimolar amounts (0.1 μM) of the five targets labeled with biotin were mixed and hybridized onto the slide for 15 min at 55°C. After hybridization, the target was revealed with streptavidin-phycoerythrin (10 min at room temperature in a dark room) and visualized by fluorescence microscopy. (**c**) and (**d**) p53 DNA interaction. (**c**) Photograph of the slide after hybridization and (**d**) quantification analysis of the slides shown in (**c**). In this experiment, equimolar amounts (0.1 μM) of unlabeled targets were hybridized, then activated p53 was applied to the slides for 30 min at room temperature. After washing, the slides were incubated with biotinylated DO7 followed by revelation with streptavidin-phycoerythrin (10 min. at room temperature in a dark room). The decrease of the curves in (**b**) and (**c**) at high probe concentrations is certainly due to steric hindrance of the streptavidin-phycoerythrin in (**b**) or the large size of the p53 tetramer complexed to two different monoclonal antibodies in (**d**). Such a decrease was not observed in the SPR analysis, as no additional molecules are needed for detection

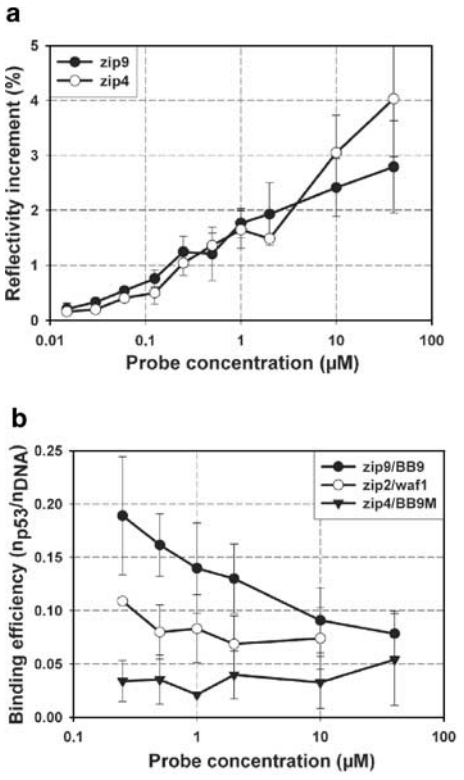

Figure 5 (**a**) Analysis of target hybridization by SPR. Contrary to fluorescence analysis, SPR analysis shows that the amount of hybridized target DNA increases with the probe concentration within the entire concentration range indicating that the system is not saturated. Each error bar corresponds to the standard deviation of two to –11 different experiments. (**b**) Binding efficiency of p53 on different target sequences. This graph shows the number of p53 molecules bound per DNA molecule for different probe concentrations. These values are calculated by determining the ratio of the reflectivity increment caused by dsDNA fixation to the increment caused by p53 fixation over two to eight different experiments

bax sequence and only a weak interaction with mdm2. Only experiments with high levels of p53 showed a significant increase of DNA binding (Figure 1). These data are supported by recent *in vivo* analyses indicating that p53 binding and transactivation via the bax response element is very weak compared to WAF or mdm2 (Inga *et al*., 2002; Qian *et al*., 2002). Furthermore, both studies showed that the transcriptional activation of WAF1 promoter by p53 is two to five times stronger than for mdm2 promoter, supporting the results of our *in vitro* studies.

Missense mutations of the p53 gene have been found in 50% of human cancer (Soussi and Béroud, 2001, 2003) and more than 1300 different p53 mutants have been reported among the 14 000 mutations listed in the p53 mutation database (Soussi and Béroud, 2003). In a recent study, Kato *et al*. (2003) constructed a library of more than 2000 p53 mutants that have been tested for transactivation with eight reporter sequences in a yeast assay. Similarly, Resnick and Inga (2003) analyzed the transactivation capacity of a series of 25 p53 mutants towards 15 promoter sequences. Both studies highlight the heterogeneous behavior of all p53 mutants. Furthermore, there is now clear evidence that some p53 mutants acquire a gain of function resulting from a specific interaction with the p73 protein leading to inhibition of the apoptotic pathway and chemoresistance (Bergamaschi *et al*., 2003; Irwin *et al*., 2003). This genetic diversity of p53 mutants will lead to a vast number of possible phenotypes that must be evaluated in order to understand tumor behavior.

Therefore, high-throughput technology for monitoring either DNA binding activity of wt p53 toward various p53 response elements, the heterogeneity of the loss of DNA binding activity or the gain of protein–protein interaction by various p53 mutants will be of importance to further our knowledge of the significance of the loss of function of mutant p53. The response of wt p53 to stress is also highly heterogeneous (Vousden and Lu, 2002). The pattern of genes transactivated by p53 differs according to the cell type, the position in the cell cycle and the nature of the stress, the pattern of genes leading to either growth arrest or apoptosis. This can be partially due to a heterogeneous accessibility of the p53 protein to various transcription promoters either via a variation in chromatin accessibility or via accessory proteins that modulate p53 activity, such as ASPP that exclusively stimulates p53 apoptotic function (Samuels-Lev *et al*., 2001). The use of a zip-code methodology to graft specific DNA sequences onto the chips allows analysis of a wide range of interactions with a similar chip. Furthermore, the pyrrole-based technology is not restricted to nucleotides and can be used for other molecules, such as small ligands, antibodies, or oligosaccharides. SPR imaging can be used for all specific macromolecular interactions. Its combination with a high-throughput methodology and the possibility of monitoring hundreds of simultaneous reactions should make it a method of choice in the study of proteome interactions (Walhout and Vidal, 2001; Drewes and Bouwmeester, 2003).

Experimental protocol

Generic single-strand DNA chip preparation

Our approach uses universal microarrays of unique 24-base oligonucleotides or zip-codes (Gerry *et al*., 1999) that are coupled to the pyrrole during synthesis. The chips were made by electrochemical copolymerization of each pyrrole-functionalized zip-code (Zip-Pyr) using the electrospotting method as previously described (Guedon *et al*., 2000). Briefly, the electrochemical cell, that is, a pipette tip with a platinum wire, was filled with a solution containing 20 mM pyrrole in a saline buffer and various concentrations of Zip-Pyr. The polypyrrole film was synthesized by electrocopolymerization (electrochemical pulse) on the gold layer (working electrode) and successive polymerizations with different Zip-Pyr on defined areas of the gold slide allow the construction of a multiparametric single-strand DNA chip (Figure 4a

and b). The zip-sequences used in our study are described in Table 1. When all Zip-Pyr spots have been synthesized, the slide is disconnected, rinsed with water, dried with a nitrogen stream, and stored at 4°C.

DNA binding reaction

Human wt p53 was overexpressed using recombinant baculovirus and analyzed by EMSA using a two-step procedure. In the first step, p53 was activated with HR231 monoclonal antibodies in the DNA binding buffer (10 mM HEPES, pH 8.0, 0.1 mM EDTA, 50 mM NaCl, 50 mM KCl, 5 mM DTT, 4 mM spermidine, 18% glycerol, 0.05% NP40, 11 μg/ml of poly-dIdC). This activation reaction was performed in a volume of 20 μl for 30 min at 20°C with 1 μg of monoclonal antibody. In the second step, 0.2 ng of labeled DNA probe was added and a second incubation for 30 min at 20°C was performed. Reaction products were loaded onto a 4% polyacrylamide gel containing 0.5 × TBE. Electrophoresis was performed for 2 h. Gels were dried and exposed to X-ray film.

For SPR analysis, p53 activation was performed in a total volume of 300 μl of modified DNA binding buffer (10 mM HEPES, pH 8.0, 0.1 mM EDTA, 50 mM KCl, 5 mM $MgCl_2$, 2 mM DTT, 4 mM spermidine, 0.2 g/l BSA, 10% glycerol, 0.05% NP40) for 30 min at room temperature (20°C). The entire volume of the activation reaction was then injected onto the chip that had been previously equilibrated with the same buffer.

SPR imaging

The system was designed and implemented using the Kretschmann configuration, in which the plasma waves at the interface between a metal and a dielectric are excited with an evanescent field created by a light beam at a particular incidence angle (see Supplementary Figure 1 online). A collimated p-polarized electroluminescent diode ($\lambda = 660$ nm) illuminates the entire functionalized gold surface coated onto the coupling prism under a variable incidence. The entire reflected beam is then directed to a 12-bit CCD camera via an optical system. This afocal optical system is quite simple because the refractive index and top angle of the prism have been optimized to improve the image quality. A home-developed program (LabVIEW®) monitors the experiments. This includes recording the images and calculating the different signal changes at several-second intervals. The transducing gold surface (48 nm thick) is placed against a Teflon cell (diameter: 8 mm, volume: 25 μl) connected to a peristaltic pump (Minipuls™) for injection. Before measuring the kinetics of the interaction on the gold surface, working buffer was injected at a rate of 25 μl/min for 30 min until the surface reached its equilibrium state. At this step, the measurement of the reflectivity around the resonance angle (data not shown) allowed precise positioning of the mirror for the kinetic measurements. The angle of incidence was then chosen at the point of maximum slope of the reflectivity dip caused by SPR. At this fixed angle, the amount of molecules bound to the probes is directly related to the reflectivity variation. Successive injections of molecules of interest in working buffer separated by rinsing with working buffer (25 μl/min) allowed real-time measurement of molecule binding in parallel over each Zip-Pyr spot at room temperature (20°C). Some kinetics, recorded in real-time and in parallel over the 25 spots, are represented in Figures 4c and d and in the Supplementary Figure 3 online.

Acknowledgements
This work was supported by grants from the Association de la Recherche sur le Cancer (TS No. 4809), Ligue Nationale Contre le Cancer (Comité de Paris), the European Community's Fifth Framework Programme (QLRT-1999-00273), and Université PM Curie to TS. DC was supported by a fellowship from the Association de la Recherche sur le Cancer.

References

Balagurumoorthy P, Sakamoto H, Lewis MS, Zambrano N, Clore GM, Gronenborn AM, Appella E and Harrington RE. (1995). *Proc. Natl. Acad. Sci. USA*, **92,** 8591–8595.

Bergamaschi D, Gasco M, Hiller L, Sullivan A, Syed N, Trigiante G, Yulug I, Merlano M, Numico G, Comino A, Attard M, Reelfs O, Gusterson B, Bell AK, Heath V, Tavassoli M, Farrell PJ, Smith P, Lu X and Crook T. (2003). *Cancer Cell*, **3,** 387–402.

Deppert W, Gohler T, Koga H and Kim E. (2000). *J. Cell. Biochem. Suppl.,* (Suppl 35)**,** 115–122.

Dong SM, Traverso G, Johnson C, Geng L, Favis R, Boynton K, Hibi K, Goodman SN, D'Allessio M, Paty P, Hamilton SR, Sidransky D, Barany F, Levin B, Shuber A, Kinzler KW, Vogelstein B and Jen J. (2001). *J. Natl. Cancer Inst.*, **93,** 858–865.

Drewes G and Bouwmeester T. (2003). *Curr. Opin. Cell. Biol.*, **15,** 199–205.

El-Deiry WS, Kern SE, Pientenpol JA, Kinzler KW and Vogelstein B. (1992). *Nat. Genet.*, **1,** 45–49.

Favis R, Day JP, Gerry NP, Phelan C, Narod S and Barany F. (2000). *Nat. Biotechnol.*, **18,** 561–564.

Fried M and Crothers DM. (1981). *Nucleic Acids Res.*, **9,** 6505–6525.

Friedlander P, Haupt Y, Prives C and Oren M. (1996). *Mol. Cell. Biol.*, **16,** 4961–4971.

Galas DJ and Schmitz A. (1978). *Nucleic Acids Res.*, **5,** 3157–3170.

Gerry NP, Witowski NE, Day J, Hammer RP, Barany G and Barany F. (1999). *J. Mol. Biol.*, **292,** 251–262.

Guedon P, Livache T, Martin F, Lesbre F, Roget A, Bidan G and Levy Y. (2000). *Anal. Chem.*, **72,** 6003–6009.

Halazonetis TD, Davis LJ and Kandil AN. (1993). *EMBO J.*, **12,** 1021–1028.

Hansen S, Hupp TR and Lane DP. (1996). *J. Biol. Chem.*, **271,** 3917–3924.

Inga A, Storici F, Darden TA and Resnick MA. (2002). *Mol. Cell. Biol.*, **22,** 8612–8625.

Irwin MS, Kondo K, Marin MC, Cheng LS, Hahn WC and Kaelin WG. (2003). *Cancer Cell*, **3,** 403–410.

Kato S, Han SY, Liu W, Otsuka K, Shibata H, Kanamaru R and Ishioka C. (2003). *Proc. Natl. Acad. Sci. USA*, **100,** 8424–8429.

Kim E and Deppert W. (2003). *Biochem. Cell. Biol.*, **81,** 141–150.
Livache T, Maillart E, Lassalle N, Mailley P, Corso B, Guedon P, Roget A and Levy Y. (2003). *J. Pharm. Biomed. Anal.*, **32,** 687–696.
Melino G, De Laurenzi V and Vousden KH. (2002). *Nat. Rev. Cancer*, **2,** 605–615.
Muller BF, Paulsen D and Deppert W. (1996). *Oncogene*, **12,** 1941–1952.
Qian H, Wang T, Naumovski L, Lopez CD and Brachmann RK. (2002). *Oncogene*, **21,** 7901–7911.
Resnick MA and Inga A. (2003). *Proc. Natl. Acad. Sci. USA*, **100,** 9934–9939.
Rich RL and Myszka DG. (2000). *Curr. Opin. Biotechnol.*, **11,** 54–61.
Rowan S, Ludwig RL, Haupt Y, Bates S, Lu X, Oren M and Vousden KH. (1996). *EMBO J.*, **15,** 827–838.
Samuels-Lev Y, O'Connor DJ, Bergamaschi D, Trigiante G, Hsieh JK, Zhong S, Campargue I, Naumovski L, Crook T and Lu X. (2001). *Mol. Cell*, **8,** 781–794.
Soussi T and Béroud C. (2001). *Nat. Rev. Cancer*, **1,** 233–240.
Soussi T and Béroud C. (2003). *Hum. Mutat.*, **21,** 192–200.
Tokino T, Thiagalingam S, El -Deiry WS, Waldman T, Kinzler KW and Vogelstein B. (1994). *Hum. Mol. Gen.*, **3,** 1357–1542.
Vogelstein B, Lane D and Levine AJ. (2000). *Nature*, **408,** 307–310.
Vousden KH and Lu X. (2002). *Nat. Rev. Cancer*, **2,** 594–604.
Walhout AJ and Vidal M. (2001). *Nat. Rev. Mol. Cell. Biol.*, **2,** 55–62.

Supplementary Information accompanies the paper on Oncogene website (http://www.nature.com/onc)